High-resolution resistance mapping in SEM

Grigore Moldovan, Wolfgang Joachimi
point electronic GmbH, Erich-Neuß-Weg 15, D-06120 Halle, Germany
grigore.moldovan@pointelectronic.com

Guillaume Boetsch
Imina Technologies SA, EPFL Innovation Park, 1015 Lausanne, Switzerland

Jörg Jatzkowski, Frank Altman
Fraunhofer Institute for Microstructure of Materials and Systems (IMWS), Center for Applied Microstructure Diagnostics, Walter-Huelse-Strasse 1, D-06120 Halle, Germany

Abstract

This work presents advanced resistance mapping techniques based on Scanning Electron Microscopy (SEM) with nanoprobing systems and the related embedded electronics. Focus is placed on recent advances to reduce noise and increase speed, such as integration of dedicated *in situ* electronics into the nanoprobing platform, as well as an important transition from current-sensitive to voltage-sensitive amplification. We show that it is now possible to record resistance maps with a resistance sensitivity in the 10Ω range, even when the total resistance of the mapped structures is in the range of 100Ω. A reference structure is used to illustrate the improved performance, and a low-resistance failure case is presented as an example of analysis made possible by these developments.

Introduction

The main motivation for the development of the resistance mapping technique in SEM originates from Electrical Failure Analysis (EFA), where a range of failure cases require resistance maps with high spatial resolution. Typical examples for semiconductor devices are localization and characterization of open and shorts, including leaky opens and highly resistive shorts, as well as for the development of built-in resistive and capacitor structures. Resistive mapping is also required for the electrical failure analysis of large area devices, such as batteries and photovoltaics, where resistance plays a key role in device performance.

Resistance mapping in SEM can be found in the literature described as Electron Beam Absorbed Current / Resistive Contrast Imaging (EBAC/RCI) [1-6] because it originates from the studies on Charge Collection (CC) or Specimen Current (SC) imaging. However, this family of related methods is even broader, as it includes a few more techniques relevant to resistance mapping, such as Electron Beam Absorbed Voltage (EBAV), as well as other techniques that do not relate directly to resistance mapping, such as Electron Beam Induced Resistance Change (EBIRCh) [7] and Electron Beam Induced Current (EBIC).

Whilst this abundance of specialized methods reflects the creative ability of failure analysts to produce new techniques when required to solve specific cases, it does also require classification for clarity. First, it is useful to identify the techniques that produce resistance data, which cover EBAC/RCI and EBIRCh. Second, it is useful to distinguish between mapping resistance behavior, i.e. EBIRCh, and mapping intrinsic resistance, i.e. EBAC/RCI.

The EBIRCh technique relies on observing resistance changes in reaction to the electron beam, and therefore provides a map of resistance behavior, not of intrinsic resistance. Further, altering the resistance of the structure investigated is only adequate in the context of localization, not when mapping of intrinsic resistance is required. Further, EBIRCh requires that a constant bias is applied, which may induce stress on the device and thus change the intrinsic resistance. Last but not least the induced electron beam current from the SEM probe influence the measured resistance change values which overlays the pure EBIRCh signal.

The EBAC/RCI technique relies on the division of the current in the resistive structure based on relative resistance in two or more probes. Measurement of these signals therefore gives a direct observation of the intrinsic resistance, and the resultant images can be calibrated in Ω units. Note that the RCI current division configuration must be used, as the more general EBAC technique does not provide the resistance contrast. EBAC/RCI has evolved from the charge collection study and is therefore a current-based technique. However, the current measurement is not the optimal approach to mapping the resistance, as the signal to noise ratio is poor for structures with reduced total resistances. For example, noise reduction performance is particularly relevant when the resistive structure to be mapped has less than 1kΩ, which is the typical case for leaky shorts. Therefore, a general resistance mapping technique must be sensitive for such small resistance structures.

This work proposes using the established signal division approach, but in a voltage-based configuration instead, which is suitable for structures with much smaller total resistance. This means that the previous current-sensitive *in situ* preamplifier is replaced with a voltage-sensitive preamplifier. The general voltage-based characterization can found in previous literatures as Electron Beam Absorbed Voltage (EBAV), therefore this new approach could be termed EBAV/RCI, in keeping with the established EBAC/RCI notation. For simplicity, the term "resistance mapping" is used as it can cover both current- and voltage-based techniques, and is explicit that the output is maps of intrinsic resistance.

This paper will present a comparison of current- and voltage-based designs, showing resistance maps from the same resistive structure with both sets of electronics. To illustrate the benefits of the improved design, a real-case application is shown for a low-resistance short in 22nm technology device that could not be localized using the conventional current-based approach.

Method & Results

Current/voltage amplification comparison

A resistance chain test structure was used to evaluate mapping performance. This test structure is a meandering chain defined between two metal layers, constructed of 8 passes of 80 segments. The total resistance of the structure is 500Ω, with 62.5Ω/pass and 0.78Ω/segment. The device was loaded on the proBee nanoprobing solution provided by Imina Technologies SA and point electronic GmbH, and equipped with a current-sensitive preamplifier. The nanoprober and sample were then loaded into an upgraded Gemini I SEM from Zeiss. A typical secondary electron image is presented in Figure 1

The upper end of the resistive structure, as presented in Figure 1, was connected to the input of the current-sensitive preamplifier, and the lower end of the resistive structure was connected to ground. - the respective resistance map is presented in Figure 2. The experiment above was then repeated using a new voltage-sensitive preamplifier.

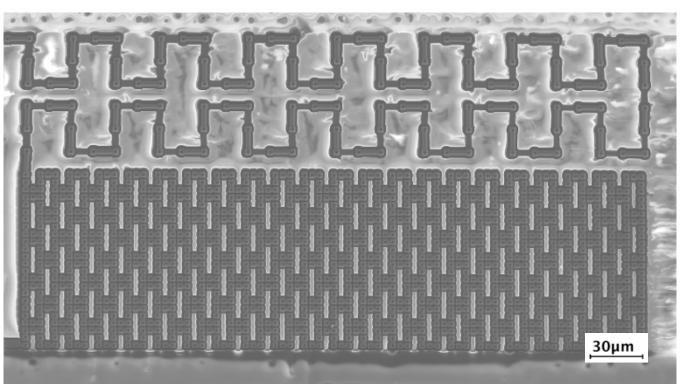

Figure 1: Secondary electron image of resistive test structure, showing in the lower part 8 passes of 80 segments

Similarly, the upper end of the resistive structure was connected to the input of the voltage-sensitive preamplifier, and the lower end to ground. The same SEM conditions were applied, including acceleration voltage and aperture. The resultant resistance map is presented in Figure 3.

Quality differences of resistance mapping are evident when switching from the current-sensitive to the voltage-sensitive amplification. This is particularly evident in areas where relative resistance to input is high (bottom right of the image) and therefore the signal after resistive division is low, see Fig.2 and 3. Improvements are found for the entire structure, even in areas where relative resistance to input is low (top right of the image), and therefore the signal after resistive division is higher. The improvements are attributed principally to an improved signal to noise ratio.

Differences in contrast are observed between the two metal layers, as a smaller percentage of the electron beam is absorbed in the deeper metal layer. This may be observed for both cases, but the improved signal to noise ratio gives an easier and more confident contrast interpretation. Evidently, a careful choice of acceleration voltage is necessary for sufficient currents to be absorbed in both metal layers, and 10kV was found suitable for this test structure.

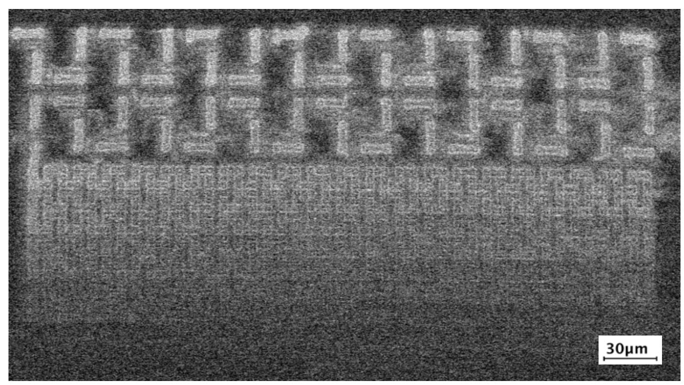

Figure 2: Resistance map recorded with current-sensitive amplification. The test structure is visible, but details are lost in the noise, as expected for a total resistance of only 500Ω

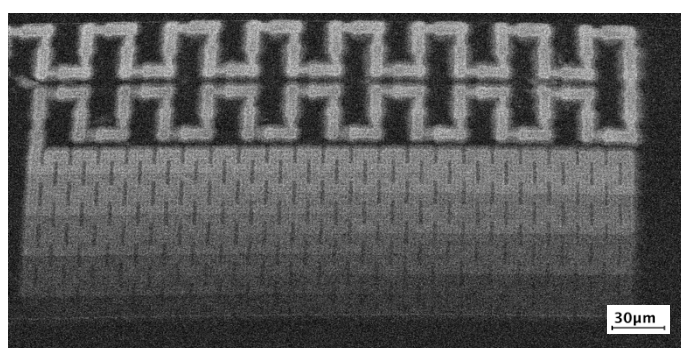

Figure 3: Resistance map recorded with voltage-sensitive amplification. The resistive chain is now clearly resolved, e.g. details at the bottom right of the image.

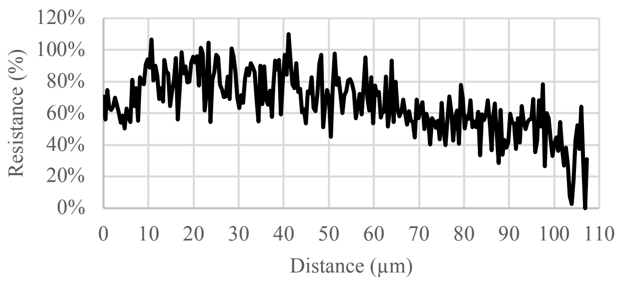

Figure 4: Line profile of resistance measured across the test structure with current-sensitive amplification. A general decrease is visible, but not the individual meanders.

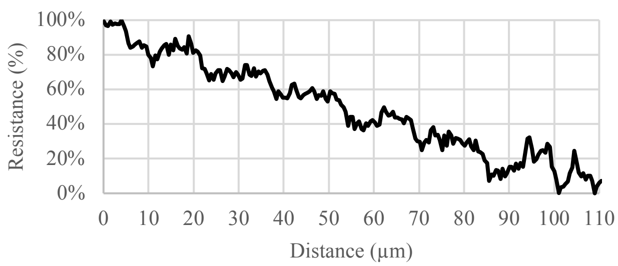

Figure 5: Line profile of resistance measured across the test structure with voltage-sensitive amplification. Details of individual meanders are now visible.

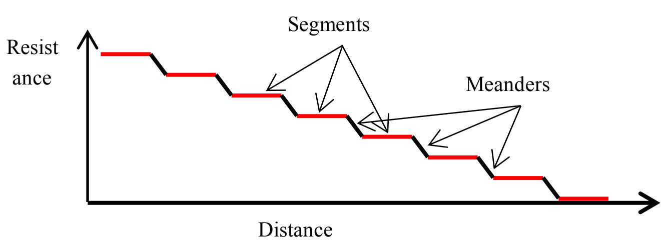

Figure 6: Schematic of expected resistance line profile across the test structure. A larger 60Ω step is expected for each meander, with a smaller 1Ω decrease for each segment.

To better illustrate the differences in resistance mapping, line profiles were recorded by scanning the electron beam across the meandering test structure (i.e. from top to bottom of Figure 1). Longer pixel dwell times were used than in Figures 2 and 3, so that details in resistance mapping are clearer. Recorded line profiles are showed in Figures 4 and 5.

By comparing the two profiles it becomes evident that the voltage-based approach not only has an improved signal to noise ratio, but also reveals detailed high-resolution resistance. The individual steps corresponding to each meander are now clearly visible as larger steps in the line profile, as they each have 60Ω. There is one segment between each these meander steps, oriented in opposite directions at each pass, but the gradient of these is less clear, as they have only 1Ω.

Failure analysis example

A failed resistance via chain is used next as an illustration of a real case. The via chain contains an open with a reduced total resistance, which prevented analysis with the current-sensitive amplification as the signal to noise ratio was poor. Voltage-sensitive amplification was chosen for resistance mapping and therefor for the localization of the failure site.

The device was loaded onto the proBee nanoprobing solution provided by Imina Technologies SA and point electronic GmbH, and equipped with a voltage-sensitive preamplifier. The nanoprober and sample were then loaded into an upgraded Gemini I SEM from Zeiss, and the corresponding contacting sites were located and probed. Figure 7 shows an SE image of the probed structure.

SEM acceleration voltage and aperture were selected to provide an adequate absorbed current in the via chain, and the lower probe from these images was connected to the input of the voltage-sensitive preamplifier. The resultant resistance map is presented in Figure 8.

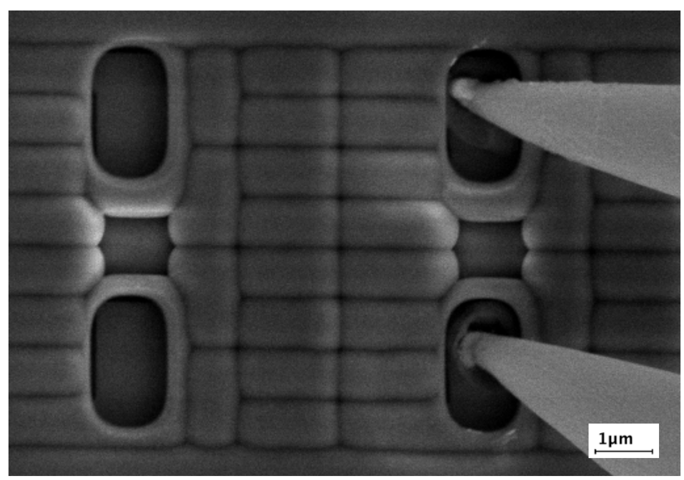

Figure 7: SE image showing probed via chain in preparation for resistance mapping.

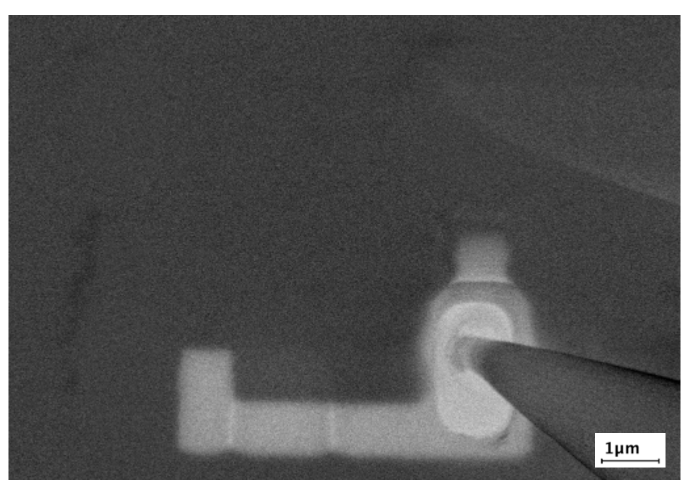

Figure 8: Resistance map using the voltage-sensitive preamplifier showing location of the open site.

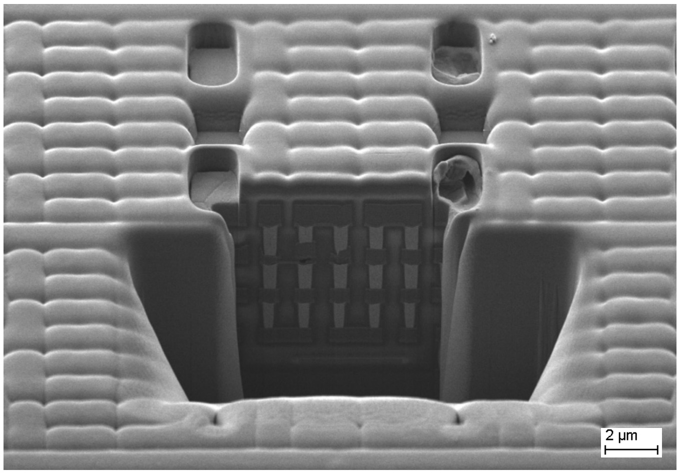

Figure 9: Overview secondary electron image showing location of the open site in the via chain, acquired at 54 degree tilt angle.

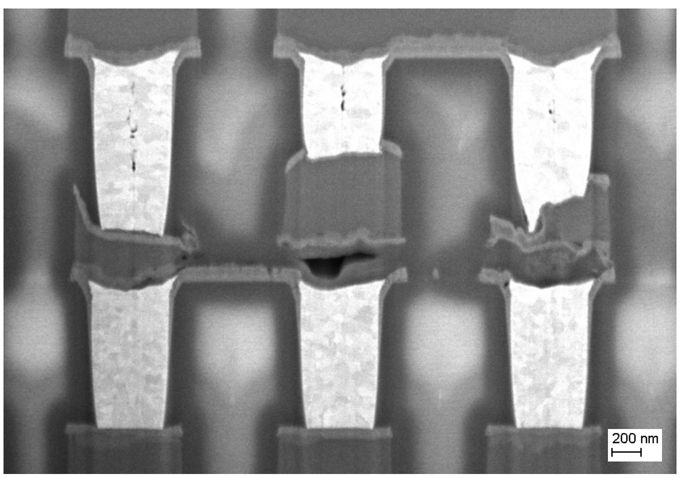

Figure 10: Cross-sectional secondary electron image showing connections at the failure site.

The resistance map clearly identifies the position at which the via chain is open, therefore the sample was transferred to a Zeiss NVision FIB-SEM for the cross-section analysis. A trench was milled to expose the buried structures. SE images of the cross-section are presented in Figures 9 - 12.

It is found that the original connection is interrupted between via 2, metal 3 and an additional connection material. This may be attributed to material remaining before barrier layer deposition after via 2 filling process. The following processing steps, including metal 3 formation, appear to have completely failed in this area, and to have resulted in the formation of an additional connection between adjacent via stacks. This additional connection at the failure site appears to have a reduced diameter, which may explain the relatively small increase in resistance observed with resistance mapping.

This failure analysis example proves that voltage-based resistance mapping could simply be integrated into the failure analysis workflow.

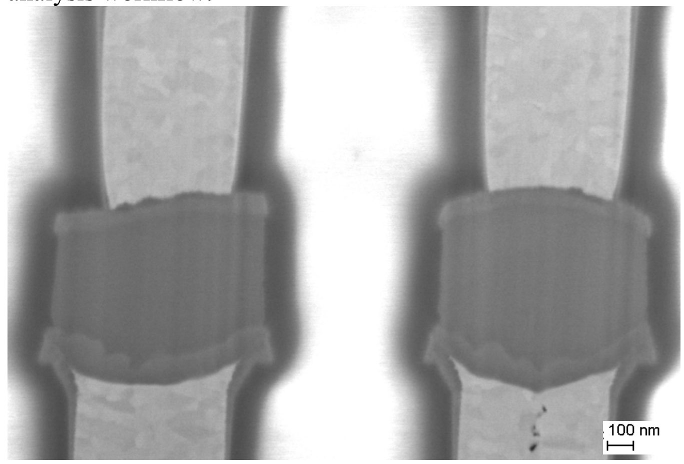

Figure 11: Detailed secondary electron image showing a reference connection

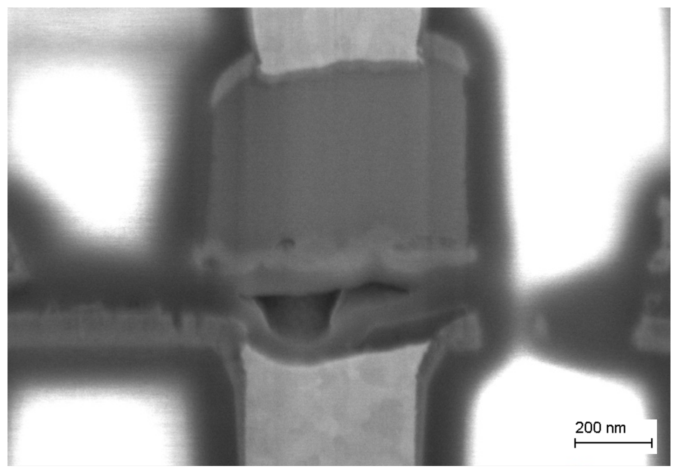

Figure 12: Detailed secondary electron image of middle via showing a residue between W plug and metal 2 structure and TiN residuals forming a short path to the adjacent via stack

Conclusions

This paper presents a brief overview of resistance related techniques in SEM, aiming to distinguish between the various approaches and acronyms. In particular, resistance mapping is distinguished from EBIRCh because of its ability to reveal resistances mapping without relying on changing the local internal resistance or applying stress on the device with a bias.

The work proposed here demonstrated the benefits of dedicated voltage-sensitive amplification for resistance mapping. It is shown that the minimum total resistance is greatly improved, from approx. 1000Ω for the case of in situ current sensitive amplification, to approx. 100Ω for the case of in situ voltage-sensitive amplification. This is important for cases where the failed structure presents a leaky open or short. Similarly, resistance sensitivity is greatly improved, reaching the 1Ω range, which is of relevance for cases where deviations in target resistance may have a large impact on device operation.

A reference via chain, and a failed resistive structure were used here to illustrate the improvements in performance, and the ease of localization with the new amplification. It is also shown that resistance mapping follows an established workflow of probing, localization and structural characterization, which makes the technique easy to apply. Finally, whilst the examples used here are CMOS devices, resistance mapping applies to any device that depends on good control of intrinsic resistances, such as MEMS, batteries, optoelectronics and photovoltaics.

Acknowledgments

This work has been (partly) performed in the project SAM3, where the German partners are funded by the *German Bundesministerium für Bildung und Forschung* (BMBF) under contract No 16ES0348. SAM3 is a joint project running in the European EUREKA EURIPIDES and CATRENE programs.

References

[1] E.I. Cole, P. Tangyunyong, C.F. Hawkins, M.R. Bruce, V.J. Bruce, R.M. Ring, et al., *Resistive interconnect localization*, ISTFA Proceedings 2001, pp. 43–50.

[2] S.J. Cho, et al., Logic *Failure Analysis 65/45nm Device Using RCI & Nano Scale Probe*, IEEE Proceedings of 16th IPFA, 2009

[3] K. Dickson, et al., *Electron Beam Absorbed Current as a Means of Locating Metal Defectivity on 45nm SOI Technology*, Conf. Proc. 36th International Symposium for Testing and Failure Analysis, Addison, Texas, USA, November 2010, pp. 413-422

[4] Simon-Najasek, et al., *A new Technique for non-invasive Short-Localisation in thin dielectric Layers by Electron Beam Absorbed Current (EBAC) Imaging*, Conf. Proc. 38th International Symposium for Testing and Failure Analysis, Phoenix, Arizona, USA, November 2012, pp. 61-66

[5] P. Larré, H. Tupin, C. Charles, R.H. Newton, A. Reverdy, *Precise localization of 28 nm via chain resistive defect using EBAC and nanoprobing*, Conf. Proc. 40th International Symposium for Testing and Failure Analysis, Houston, Texas, USA, 2014, pp. 67–70.

[6] Jatzkowski, et al., Localization of weak points in thin dielectric layers by Electron Beam Absorbed Current (EBAC) Imaging, Conf. Proc. 40th International Symposium for Testing and Failure Analysis, Houston, Texas, USA, 2014, pp. 500-505

[7] Buchea, et. al., High Resolution Electron Beam Induced Resistance Change for Fault Isolation with 100nm2 Localization, Conf. Proc. 41th International Symposium for Testing and Failure Analysis, Portland, Oregon, USA, 2015. pp. 387-392